NASA TECHNICAL NOTE

NASA TN D-4066

NASA TN D-4066

EXPERIMENTAL INVESTIGATION OF LIQUID SURFACE MOTION IN RESPONSE TO LATERAL ACCELERATION DURING WEIGHTLESSNESS

by William J. Masica

Lewis Research Center

Cleveland, Ohio

NATIONAL AERONAUTICS AND SPACE ADMINISTRATION • WASHINGTON, D. C. • JULY 1967

NASA TN D-4066

EXPERIMENTAL INVESTIGATION OF LIQUID SURFACE MOTION IN RESPONSE TO LATERAL ACCELERATION DURING WEIGHTLESSNESS

By William J. Masica

Lewis Research Center
Cleveland, Ohio

NATIONAL AERONAUTICS AND SPACE ADMINISTRATION

For sale by the Clearinghouse for Federal Scientific and Technical Information
Springfield, Virginia 22151 – CFSTI price $3.00

EXPERIMENTAL INVESTIGATION OF LIQUID SURFACE MOTION IN RESPONSE TO LATERAL ACCELERATION DURING WEIGHTLESSNESS

by William J. Masica

Lewis Research Center

SUMMARY

As a part of the general study of liquid behavior in weightlessness, an experimental investigation was conducted to determine large amplitude liquid-vapor interface motion in cylinders in response to a constant lateral or transverse acceleration. With an effectively zero axial Bond number and using liquids with static contact angles near 0^{o} on the surfaces of the containers, the liquid-vapor interface was highly curved prior to the application of the lateral acceleration. The magnitude of the constant lateral acceleration ranged from 22 to 335 centimeters per second squared, each lateral acceleration having a time duration generally greater than one-half the period of fundamental free surface oscillation. The results of the investigation are correlated in terms of a defined lateral Bond number, a dimensionless parameter indicating essentially the influence of the lateral acceleration relative to the capillary forces. For no measurable dynamic contact angle, interface motion is stable (bounded in amplitude) for lateral Bond numbers less than 1.25 ± 0.05. Empirical correlations in terms of known system parameters are presented describing the observed steady interface motion in the lateral Bond number region from 3 to 100. Viscosity is included in the correlations. Qualitative results of interface behavior following the removal of the lateral acceleration and observed instances of surface instability are also presented.

INTRODUCTION

The problems associated with liquid-vapor systems in a weightless or zero-gravity environment have generated considerable interest due to the use of liquid propellant systems in space vehicle design. Excellent review articles presenting the current state-of-the-art on the physical aspects of low-gravity phenomena are found in references 1 to 4. A knowledge of the location of the liquid-vapor interface is necessary to ensure efficient venting characteristics and reliable restart capabilities during multiburn space missions. In addition, the control and stability of the vehicle flight are directly dependent

on the dynamic behavior of the propellant under all gravitational environments, ranging from the powered phase to the coast phase of the flight. Various disturbances, resulting from orientation maneuvers, attitude control thrustors, shutdown transients, etc., in space vehicle operation will occur, in general, at all angles to the vehicle thrust axis and will tend to affect adversely the desired location of the liquid-vapor interface as well as generate moments of unknown magnitude.

Only a few articles have been published describing the behavior of the interface under various forms of acceleration disturbances. The mode of liquid flow and empirical correlations governing the velocity of the interface have been obtained for the particular case where a constant acceleration is directed parallel to the longitudinal axis of a cylinder (ref. 5). Numerical studies of viscous, large amplitude surface motion starting from an initial plane surface (ref. 6) have been conducted. However, no literature relating to the low-gravity, or more properly, low Bond number (essentially, the ratio of acceleration to capillary forces) environments has been published. Although work is being done in this area, the analytic problems in describing the gross motion of a highly curved interface meeting a low contact angle boundary condition currently appear very difficult.

This report presents the results of an experimental investigation conducted at the NASA Lewis Research Center of large-amplitude liquid surface motion in a cylinder in response to a pure lateral or transverse acceleration. The phrase, pure lateral acceleration, means herein that the only effective disturbance acting on the system is a constant acceleration applied parallel to the radius of the cylinder and of duration generally longer than the half-period of fundamental free surface oscillation (as given in ref. 2). The cylinder is further constrained to move only in the direction of this lateral acceleration so that rotational disturbances are not present. The effect of the lateral acceleration is expressed in the form of a defined lateral Bond number.

The effective normal gravitational acceleration was kept below $10^{-5}g_o$ by the use of a drop-tower facility. With the range of cylinder radii (less than 3.17 cm) and specific surface tensions (greater than 11 cm^2/sec^3) used in this investigation, the axial Bond number in these very low acceleration environments was less than 0.01 and may, therefore, be regarded as effectively zero. Prior to the application of the lateral acceleration, a period of time was allowed for the interface to form its zero axial Bond number configuration. Solid-liquid-vapor systems were restricted to those having near zero static contact angles which then resulted in an initially highly curved liquid-vapor interface.

The criterion for a stable (i.e., bounded in amplitude) interface at the given conditions is presented in the form of a critical lateral Bond number. The results of this investigation are an extension of the normal gravity investigation presented in reference 7. Empirical relations describing the steady motion of the interface leading edge and the defined steady vapor-penetration velocity due to lateral Bond numbers greater than critical are presented in terms of dimensionless parameters that are generally applicable

to right circular containers. The effect of viscosity is included in the correlations governing the steady liquid-vapor interface motion. Observations of anomalous interface behavior and the effect of acceleration cutoff are also qualitatively discussed.

SYMBOLS

a	axial acceleration, cm/sec^2
a_L	lateral acceleration, cm/sec^2
Bo	axial Bond number, $Bo = aR^2/\beta$
Bo_L	lateral Bond number, $Bo_L = a_L R^2/\beta$
g_o	acceleration due to gravity, 980 cm/sec^2
h	maximum interface extension (see fig. 5), cm
K	dimensionless frequency parameter constant
K_o, K_L	empirical constants at given lateral bond numbers
R	cylinder radius, cm
r	radial location of maximum vapor penetration point X_o, cm
Re	Reynolds number, $Re = \rho R V_L/\eta$
t	duration of lateral acceleration, sec
T_0	fundamental period of interface, sec
V_L	steady interface leading-edge velocity, cm/sec
V_0	steady vapor-penetration velocity, cm/sec
X_L	interface leading-edge displacement (see fig. 5), cm
X_0	point of maximum vapor penetration (see fig. 5), cm
β	specific surface tension, σ/ρ, cm^3/sec^2
η	liquid viscosity, cP
ρ	liquid density, g/cm^3
σ	surface tension, dynes/cm
ω_0	natural frequency, rad/sec

APPARATUS AND PROCEDURE

Test Facility

To provide the proper environmental conditions, that is, an effectively zero axial Bond number, the experimental investigation was conducted in the Lewis Research Center drop tower. This facility provides a usable drop distance of 85 feet or approximately 2.3 seconds of unguided free fall. The resultant acceleration due to air drag on the experiment package is kept below $10^{-5} g_o$ by allowing the package to free-fall inside a protective drag shield, designed with a high weight-to-frontal area ratio and low drag coefficient. A schematic of the facility is shown in figure 1.

Experiment Package

The lateral acceleration of the cylinder was obtained by using a series of constant-force springs mounted on the experiment package with tensions ranging from 0.12 pounds (5.5×10^4 dynes) to a maximum nominal value of 1 pound (4.5×10^5 dynes). Nonuniform wrapping and jerking were largely eliminated by mounting the drum of the force springs at a slight angle with respect to the applied tension direction. The force-spring tension was supplied through a lightweight cable of neglible mass to a carriage holding the test cylinder. For those data runs requiring acceleration cutoff, a small plastic clip was fastened on the cable. The position of the clip determined the net accelerated time of the carriage. A solenoid controlled air piston was used to position the carriage under tension prior to the desired release time. The carriage rode on two case hardened, 3/8-inch (0.95-cm) diameter shafts and was supported by a three-point precision bushing assembly. Accurate parallelism of the shafts and zero play were ensured by line boring the shaft mounts and splitting the carriage assembly to permit adjustment for proper alinement. Measured 1-g coefficients of static and rolling friction of the slide assembly were less than 0.005, resulting in negligible friction effects over the range of accelerations used in the investigation. Precision diameter borosilicate glass and polished acrylic plastic cylinders with radii ranging from 0.317 to 3.17 centimeters were rigidly mounted on the carriage and alined perpendicular to the travel direction. The entire slide assembly was placed in a box having a dull white interior and indirect illumination to allow a fixed 16-millimeter high-speed motion-picture camera to photograph the liquid behavior and the total carriage travel. The length of travel was dictated by the experiment package dimensions and the desire to view the entire carriage displacement. Through the use of wide angle lenses, approximately 22 centimeters of viewable travel could be obtained in this investigation. A photograph of the experiment package is given in figure 2.

Test Liquids

The liquids and their physical properties pertinent to this investigation are presented in table I; handbook values are given where available. The surface tensions of trichlorotrifluoroethane and the glycerol mixture were measured by using the ring method with a Du-Nouy tensiometer and appropriate ring correction factors. Viscosity measurements of these same liquids were made by using a rolling-ball-type viscosimeter. All liquids were analytic reagent grade and exhibited static contact angles very near 0° on the surface of the containers. A small quantity of dye was added to each liquid to improve photographic quality, the addition of which had no measurable effect on the liquid properties.

Operating Procedures

Contamination of the liquids and cylinder surfaces, which could alter the liquid properties and contact angles of the test liquids, was carefully avoided. To ensure perfect wetting, ultrasonic cleaning procedures were used. Because the acrylic plastic cylinders were particularly susceptible to crazing with the test liquids used, periodic heat treatment and repolishing were necessary.

After the cylinders were filled to the desired height with the test liquids and mounted on the carriage, the experiment package was placed inside the drag shield. Initiation of free fall was accomplished by pressurization of an air cylinder that forced a knife edge into a support wire fixed to the drag shield assembly causing the wire to fail. The application of the lateral acceleration (by releasing the air piston holding the carriage) was

TABLE I. - SUMMARY OF LIQUID PROPERTIES

[Properties at 20° C]

Liquid	Surface tension, σ, dynes/cm	Density ρ, g/cm^3	Specific surface, β, cm^3/sec^2	Viscosity, η, g/(cm-sec)
Ethanol	22.3	0.789	28.3	0.012
Trichlorotrifluoroethane	18.6	1.58	11.8	.007
Methanol	22.6	.793	28.5	.006
Carbon tetrachloride	26.9	1.59	16.8	.0097
1 - Butanol	24.6	.809	30.4	.029
60 Percent ethanol - 40 percent glycerol[a]	26.9	.988	27.2	.154
Acetone	23.7	.792	29.9	.0032

[a]Percentage composition by volume.

preceded by a time delay to allow the liquid-vapor interface to form its zero axial Bond number configuration. This time was generally not sufficient to ensure the complete absence of oscillatory interface motion, but represented, for the range of cylinder radii and liquid properties used, a compromise between an adequate formation period and a sufficient time in the lateral acceleration field to observe the dynamic behavior of the interface. Disturbances supplied to the experiment package during free fall due to the reaction of the force-spring system were negligible because of the large mass ratio involved. In this same regard, it should be noted that the liquid motion (including the oscillatory behavior following acceleration cutoff) had no measurable effect on the carriage displacement characteristics, again because of the large ratio of the carriage and cylinder assembly mass to the effective liquid mass. Prior to deceleration in a sandbed, the package came to rest on the bottom of the drag shield, resulting in a usable test time of about 2.2 seconds. A schematic illustration of a test drop sequence is shown in figure 3.

DATA REDUCTION

All data were recorded photographically and analyzed with the aid of a motion-picture film reader. Time measurements were obtained by viewing a digital clock with calibrated accuracy of 0.01 second. Measurements were corrected, when required, for refraction and parallax error.

The magnitude of the lateral acceleration was directly measured in each run by observing as a function of time the carriage displacement along a ruler placed parallel to the shafts. Accurate starting time indication of the lateral acceleration is necessary as this value significantly affects the initial displacement characteristics. In this investigation, starting time was obtained by a neon bulb trace along the side of the data film, electrically actuated by the physical release of the air piston to the carriage. A typical set of log displacement against log time points is shown in figure 4. A curve was fitted to these points by using a constant slope of 2; the acceleration value was then obtained from an appropriate intercept of the curve. Although the initial displacement was not, in general, parabolic in time (e.g., fig. 4), forcing the slope value was consistent with the major portion of the actual displacement characteristics so that a constant acceleration could be legitimately assumed. For those data runs requiring acceleration cutoff, the continuous measurement of carriage displacement in time further established that the carriage continued at constant velocity after acceleration cutoff. The magnitudes of the lateral accelerations used in this study ranged from 22.2 to 335 centimeters per second squared and were determined by the given procedure to within 5 percent.

PRELIMINARY DEFINITIONS

Bond Number Parameter

The Bond number parameter is a dimensionless quantity indicating the relative importance of gravitational and capillary forces. This parameter is used to describe the static equilibrium interface configuration (e.g., ref. 2) and as a convenient scaling parameter to establish dynamic flow regimes (ref. 5). In a cylinder, the Bond number is defined as

$$Bo = \frac{aR^2}{\beta} \tag{1}$$

where the density of the vapor phase has been neglected. In this investigation, the axial Bond number is effectively zero because of the chosen combination of liquid properties, cylinder radii, and net acceleration level obtained in a drop-tower facility. When coupled with solid-liquid-vapor combinations producing static contact angles near 0^o, this zero axial Bond number resulted in an initially highly curved interface prior to the application of the lateral acceleration. An illustration of the case under investigation is shown in figure 5.

In previous investigations (e.g., ref. 7), it has been shown that there exists a critical value of the Bond number separating an unstable and stable interface under constant accelerations. Unstable, as used herein, means only that inviscid interface motion due to the applied acceleration is unbounded in amplitude, and does not necessarily imply surface instabilities (resembling Taylor or Helmholtz instabilities) or breakup of some steady flow condition. A stable interface means that the interface motion under a constant acceleration is bounded in amplitude. The critical value of the Bond number is a function of the interface configuration (i.e., container geometry and contact angle) and the direction of the applied acceleration with respect to the liquid-vapor interface. For an initially highly curved liquid-vapor interface, cylindrical geometry, and 0^o static contact angle, the critical Bond number is 0.84 for constant accelerations directed parallel to the longitudinal axis of the cylinder.

Lateral Bond Number

Equation (1) refers only to constant accelerations directed along the longitudinal axis of a cylinder. For that special case where the only effective acceleration is directed along the radius of the cylinder and where the system is constrained to move only in the direction of this acceleration, one may define a lateral or transverse Bond number

$$Bo_L = \frac{a_L R^2}{\beta} \tag{2}$$

where a_L is the magnitude of the applied lateral acceleration. This definition is a convenient parameter describing the influence of the lateral acceleration relative to the surface energy on the nehavior of the liquid-vapor interface. The usefulness of this definition will rest, of course, on its ultimate applicability. The constraint condition on the motion of the system precludes rotational effects produced by the changing liquid center of mass.

The critical lateral Bond number defines the region between a stable and unstable interface under constant lateral accelerations. It can be shown that this critical lateral Bond number, for static equilibrium, 0^o contact angle systems should be on the order of one. A variational approach for a two-dimensional system along with generated interface profiles is given in reference 8. Some experimental results in this area with normal gravitational acceleration in small radii cylinders are given in reference 7. A critical lateral Bond number of 1.12 is given with a higher value for $\beta > 43$ cubic centimeters per square second. In retrospect, this higher value may have been caused by inducing a finite contact angle while rotating the test cylinder to a horizontal position. Contact angle changes, introduced by flow, surface roughness, aging, etc., will affect the observed critical Bond number.

Time Duration of Lateral Acceleration

In order to distinguish the lateral acceleration from an impulsive type disturbance (which is not implied in the lateral Bond number definition), an adequate criterion of acceleration time duration must be applied. It is recognized that the acceleration time should be much greater than the period of fundamental free-surface oscillation, but because of available experimental time, such conditions are not always possible. The time criterion generally applied in this investigation was that the acceleration time must be greater than the half-period of fundamental interface oscillation.

An approximation to the asymmetric natural frequency of the interface for zero axial Bond numbers and 0^o contact angles with no hysteresis is suggested in reference 2:

$$\frac{\omega_0^2 R^3}{\beta} = K \tag{3}$$

where K is 1.5. (Unpublished NASA data suggest that the constant K should be

about 2.6, but for this investigation the quoted value will suffice.) The criterion for the minimum time duration of the lateral acceleration is

$$t > \frac{T_0}{2} = \pi \left(\frac{R^3}{1.5\,\beta} \right)^{1/2} \tag{4}$$

RESULTS AND DISCUSSION

Critical Lateral Bond Number

The first phase of this investigation was directed toward establishing the magnitude of the critical lateral Bond number. The method used was to observe stable and unstable interface motion in various diameter cylinders as a function of lateral acceleration and liquid properties. Practical criteria of stable and unstable motion involved observations based on at least one diameter of net interface motion. Data where the maximum interface extension h was less than 3R and where the leading-edge and vapor-penetration velocities (V_L and V_0 in fig. 5) were definitely zero were selected to be representative of stable motion. Conversely, unstable motion meant $h/R > 3$ and positive leading-edge and vapor-penetration velocities (i.e., in the directions shown in fig. 5). These criteria are consistent with the definition of the critical lateral Bond number and the limited analytical work in this area (ref. 8) and are identical to the criteria used in a previous experimental investigation (ref. 7).

Solid-liquid-vapor combinations had near 0° static contact angles, verified by observing the equilibrium zero axial Bond number interface configuration. To eliminate the possibility of introducing a dynamic contact angle at the advancing leading edge (refs. 9 and 10), the less viscous fluids given in table I were used (butanol and ethanol-glycerol were omitted). Parameters were chosen to create interface velocities as small as possible. Under these conditions, no measurable dynamic contact angles were observed in the critical lateral Bond number region.

With the given criteria, the stable and unstable data were plotted in the form shown in figure 6. For these data the liquid height from the bottom of the cylinder was at all times greater than 1 diameter. The zero axial Bond number interface configuration prior to the application of the lateral acceleration was effectively quiescent and hemispherical. The lateral acceleration time exceeded that given by equation (4). Over the range of parameters used, no surface instabilities were observed in this lateral Bond number region. The several points obtained in the normal gravity investigation where the observed stable interface was continuously smooth (fig. 4 in ref. 7) are included in figure 6.

A hand-fit constant-slope (exponent) curve was used to separate the stable and unstable data in figure 6. The slope of this line indicates that a critical lateral Bond number can be used to delineate the stable and unstable regions. The value of this critical lateral Bond number, obtained from the curve at a convenient intercept, is 1.25±0.05.

For the stable data points, or for lateral Bond numbers less than critical, the leading-edge and vapor-penetration velocities were, of course, highly nonlinear and no attempt was made to correlate dynamic motion. In addition, it is noted that the leading-edge has a tendency, in many cases, to overshoot its final stationary height, receding in a draining fashion along the cylinder wall. Because of this, quantitative height-rise measurements, especially in cylinders of the size range used, are difficult to make. For very small (<0.4) lateral Bond numbers, where the change from a zero axial Bond number configuration is small and the dynamic motion is symmetric, the interface was observed to oscillate.

Lateral Bond Numbers Between Critical and 3

In the lateral Bond number region above critical but approximately less than 3, the interface displacements X_L and X_0 were generally nonlinear, decaying exponentially in time. Reynolds numbers, however, based on the maximum measurable leading-edge velocity and cylinder radius, were quite small, being generally less than 300. In this region, and especially for Reynolds numbers less than 100, there were instances where the final observed interface configuration was stationary. The maximum interface extensions h in these latter runs were considerably greater than $3R$ and the stable motion was attributed solely to large viscous effects. The location of the maximum vapor penetration X_0 was in all instances well above several diameters from the bottom of the cylinder.

Lateral Bond Numbers Greater Than 3

Steady large amplitude interface motion. - For lateral Bond numbers in the approximate range from 3 to 100, where the Reynolds number varied from roughly 100 to 16 000, steady interface motion was observed in all instances. Steady interface motion is defined as linear displacements in time (following an initial transient) for the interface stationary points X_L and X_0. The interface displacements during steady motion were necessarily of large amplitude and were measured over distances of at least $3R$. In the large majority of data acquired in this region, the lateral acceleration time criterion given in equation (4) was met. Although it was not possible to hold to this criterion for some of the higher lateral Bond numbers, it appeared that the flow velocities created by lateral Bond

numbers of large magnitude (typical velocities were greater than 20 cm/sec) in the cylinders used in this investigation effectively dominated any natural free surface motion.

A series of photographs illustrating typical interface behavior in this lateral Bond number region is given in figure 7. In this representative run, a lateral Bond number of 3.7 is applied to a reasonably quiescent hemispherical interface obtained by allowing 0.90 second for formation. The actual lateral acceleration characteristics for this run were previously presented in figure 4. The cylinder (rad., 1.75 cm) contains methanol. Leading-edge and vapor displacements are plotted in figure 8 as a function of real time from start of the drop. The velocities V_L and V_0, for the respective leading-edge and vapor-penetration points on the interface, are indicated by the linear displacement rates and are typical of the large amplitude steady motion observed in this region.

The steady interface velocities remained measurably unaffected by the flat bottom of the cylinder until the vapor penetration reached a depth from the bottom of 0.5 R. Beyond these small depths, the vapor-penetration velocity was generally observed to decrease. It is further noted that, for initial liquid fillings where the minimum point on the interface was less than 0.5 R from the bottom, steady interface motion was not obtained.

At the higher leading-edge velocities (on the order of 15 cm/sec or more) and especially with the more viscous liquids, a small number of runs exhibited large contact angle variations in the advancing leading edge of the interface. These dynamic contact angles caused no discernible effect on interface motion other than a slight thickening of the leading edge.

Transient region. - Immediately following the application of the lateral acceleration, the interface displacements accelerated at a rate slightly less than the lateral acceleration until steady motion was reached. In this program, the transient region rarely existed beyond leading-edge displacements of 1 radius. The results in the transient region are, of course, influenced by the lateral acceleration characteristics, but a comparison of the cylinder displacement and interface displacement in each run showed nearly identical time dependence. During this transient region, the asymmetric location of the maximum vapor penetration point X_0 (located by r in fig. 5) was established.

Correlation of steady interface velocities. - An attempt was made to correlate the steady interface velocities V_L and V_0 in the form of simple dimensionless parameters as a function of lateral Bond number. The results obtained by using the parameter $V_L(R/\beta)^{1/2}$ for the measured leading-edge velocities are shown in figure 9. The spread of the points is attributed to a strong viscous effect as indicated by the fact that calculated Reynolds numbers for these points show a progressive decrease from a mean curve drawn through the data in a given lateral Bond number region. Actual Reynolds numbers, based on measured leading-edge velocity and cylinder radius, ranged from 80 to 16 000. In view of the range of radii used (0.317 to 3.17 cm) and the profile of the interface (e.g., fig. 7(d)), it is not too surprising that some form of viscous correction is required.

Various viscous correction factors were tried with a view toward simplicity and reasonableness, including a small correction for the larger Reynolds numbers. The form chosen as the most satisfactory (although certainly not unique) is given by $(1 + 7/Re^{1/2})$. Figure 10 shows the effect of applying this correction factor to the dimensionless leading-edge parameter $V_L(R/\beta)^{1/2}$.

The measured vapor-penetration velocities are seen in figure 10 to be satisfactorily represented by the dimensionless vapor-penetration parameter $V_0(R/\beta)^{1/2}$. While some viscous effects were also noted in these data, the point spread indicates that these effects over the range of variables used are relatively small, approaching accumulative measurement error. The lack of a strong viscous dependence in comparison to the leading-edge data is attributed to the radial location r of the maximum vapor penetration.

The two curves in figure 10 were hand drawn through the data and describe the interface velocities V_L and V_0 to about 10 percent, the accuracy increasing with the larger lateral Bond numbers. The form of the two curves parallel each other, which is consistent with the volume conservation during steady motion. Strong capillary effects are evident below lateral Bond numbers of about 8. The empirical correlations represented by these two curves can be used to predict the steady interface velocities. If

$$V_L\left(\frac{R}{\beta}\right)^{1/2}\left(1 + \frac{7}{Re^{1/2}}\right) = K_L$$

and

$$V_0\left(\frac{R}{\beta}\right)^{1/2} = K_0$$

then,

$$V_L = \frac{\left\{\left[4K_L(\sigma R\rho)^{1/2} + 49\eta\right]^{1/2} - 7(\eta)^{1/2}\right\}^2}{4R\rho} \tag{5}$$

and

$$V_0 = K_0\left(\frac{\beta}{R}\right)^{1/2} \tag{6}$$

where K_L and K_0 are empirical constants obtained from the leading-edge and vapor-penetration curves, respectively, at given lateral Bond numbers. The expression for V_L as given is general but will ordinarily simplify for most combinations of parameters.

Expressions for V_L and V_0 which eliminate graphical solutions can be found, but generally involve additional empirical constants. One set of these equations that satisfac-

torily describes the data is

$$\left[V_L\left(\frac{R}{\beta}\right)^{1/2} + 1.5\right]\left(1 + \frac{7}{Re^{1/2}}\right) = 2.1(Bo_L)^{1/2} \tag{7}$$

$$\left[V_0\left(\frac{R}{\beta}\right)^{1/2} + 1\right] = 0.8(Bo_L)^{1/2} \tag{8}$$

where $3 < Bo_L < 100$. For lateral Bond numbers greater than 8 and for low viscous fluids (more properly, where the Reynolds number is sufficiently large such that the viscous correction term is near unity), the form of these equations reduces to solutions of the linear portions of the curves in figure 10. It is interesting to note that, under these same conditions, equations (7) and (8) yield

$$V_L \approx 2.6\, V_0$$

which agrees with each data run.

Radial Location of Maximum Vapor Penetration

The radial or horizontal location r of the maximum vapor-penetration point X_0 on the interface was found to be determined by the magnitude of the lateral Bond number. At large lateral Bond numbers, for example, where the interface is relatively flat, the vapor-penetration point is near the cylinder wall. The radial location was measured after steady motion or a stationary interface (in the case of lateral Bond numbers less than critical) had been obtained. Results of a number of these measurements, corrected for refraction and averaged over comparable lateral Bond numbers, are presented in figure 11. Refraction correction included, where required, the location of the cylinder with respect to the normal viewing axis of the camera. Although individual measurements are subject to large error (compounded by the use of wide-angle lenses and refraction corrections), the averaged data points display a smooth trend through the range of lateral Bond numbers. The possible error in the points of figure 11 is greatest at the higher lateral Bond numbers (>30), where the ratio of radial location to radius is approaching 1 and the refraction angle is approaching critical. Note that, for the liquids used, viscosity was found to be unimportant. Near the critical lateral Bond number (1.25), the ratio of radial location to radius is about 0.5, which coincides with the two-dimensional profiles generated in reference 8.

Liquid Behavior Following Lateral Acceleration Cutoff

Removing the lateral acceleration allows the interface to return to its initial static configuration. The recovery of the interface consisted basically of large-amplitude, highly damped fundamental oscillations. Two representative runs illustrating the recovery of the interface and the start of the slosh mode are shown in figures 12 and 13. The first photographs in each figure are at acceleration cutoff and the last two are about 0.2 second into the recovery. For initially applied lateral Bond numbers above critical, the leading edge continues at a decaying rate along the cylinder wall. (Below the critical lateral Bond number, where the interface is stable, these gross inertia effects were not observed.) This initial amplitude rise drains into the major portion of the liquid, leaving a slowly decaying thin layer of liquid on the wall (e.g., fig. 12(b)). The remaining portion of the interface begins bounded oscillatory motion. In all instances, the vapor-penetration velocity responded abruptly to the termination of the lateral acceleration, even at the higher lateral Bond numbers.

The decay of the residual liquid from the wall of the cylinder produces a measurable change in liquid volume and equilibrium position of successive oscillations. Initial interface oscillations were asymmetric and aperiodic, displaying an increasing frequency. While quantitative data could not be obtained because of environmental time limitations, it was apparent that the instantaneous depth and decay of the residual liquid is an important characteristic in correlating large amplitude oscillatory interface motion.

Interface Instability

Steady, well-behaved surface motion (where the changing interface profile remained smooth) was observed in all instances where the lateral acceleration was applied to an initially quiescent, highly curved interface. Interface instability, resembling the classic Taylor form, could be generated quite easily, however, by simply applying the lateral acceleration during the initial gross formation phase (e.g., by applying the lateral acceleration a few tenths of a second after the test drop release). In these instances, the zero axial Bond number formation mode represents a perturbation on the liquid surface which grows in time during the application of the lateral acceleration.

In several instances, it was observed that even initially highly curved, well-formed interfaces (though not quiescent and displaying measurable initial velocities) also displayed surface instability of essentially the same form. The instability consisted of a single liquid column or spike growing out of the liquid surface and progressing parallel to the leading-edge displacement. In general, the instability growth rate was much greater than the leading-edge displacement rate; eventually, after several cylinder

diameters motion, the instability column collapsed into the wall creating a new nonsymmetric leading-edge pattern. A representative series of photographs showing the growth of this instability is given in figure 14. In this run, trichlorotrifluoroethane in a cylinder of radius 2.54 centimeters is subjected to a lateral acceleration of 280 centimeters per second squared. A mirror on the right of the photographs shows that the instability is symmetric with respect to acceleration direction and is not, for example, the actual leading-edge profile positioned on the far side of the cylinder.

Because of environmental time limitations, it was not possible to correlate instability occurrence, or more importantly, to determine whether formation effects alone cause this form of instability. Although instabilities were not observed when the interface was initially quiescent, the question remains as to whether larger acceleration magnitudes than available in this investigation would have, in fact, generated similar results. In this same regard, it should be noted that the accelerations required to produce instability of a highly curved, nonquiescent interface were quite large and because of limited travel distances (in terms of the time requirement given by eq. (4)) are more properly large impulsive type disturbances. No simple impulsive relation was apparent in predicting instability.

The instability data occurred generally over the range of parameters available, although never below calculated lateral Bond numbers of 12 (maximum usable radius of 1.75 cm). In view of the impulsive lateral disturbance, this lateral Bond number calculation (by eq. (2)) may be misleading, but it could indicate the upper limit of the stabilizing effect of capillarity. Qualitatively, it is interesting to note that large dynamic contact angles were always observed in runs exhibiting instability. Viscosity also appears to be most important and (when coupled with the dynamic contact angle in a no-slip boundary condition) may be the generating source of the instability. Although bottom effects make the column growth more predominant, the results indicate that instability is certainly not a result of bottom proximity alone.

SUMMARY OF RESULTS

An experimental investigation of liquid surface motion in cylinders in response to a constant lateral acceleration was conducted. With an effectively zero axial Bond number and liquids exhibiting static contact angles near 0° on the container surface, the liquid-vapor interface was highly curved prior to the application of the lateral acceleration. Using a defined lateral Bond number as a parameter in the investigation yielded the following results:

1. For no measurable dynamic contact angle variation, the interface motion is stable (bounded in amplitude) under lateral Bond numbers less than 1.25 ± 0.05.

2. For lateral Bond numbers approximately between 1.25 and 3, the interface motion is generally nonsteady with viscous effects predominating.

3. Steady interface motion exists in the lateral Bond region from approximately 3 to 100 (the limit of this investigation) for Reynolds numbers greater than 100. The steady leading-edge and defined vapor-penetration velocities are empirically correlated in terms of dimensionless parameters generally applicable to right circular containers.

4. The radial location of the defined vapor-penetration point is determined by the magnitude of the lateral Bond number.

5. Interface instability can be generated by applying a lateral acceleration to an initially nonquiescent but highly curved interface.

Lewis Research Center,
National Aeronautics and Space Administration,
Cleveland, Ohio, March 1, 1967,
124-09-03-01-22.

REFERENCES

1. Yeh, Gordon C. K.; and Hutton, Robert E.: Fluid Mechanics at Low Gravity Environments. Rep. No. 9840-6005-RU-000, TRW Space Technology Laboratories, Dec. 1964.

2. Reynolds, W. C.; Saad, M. A.; and Satterlee, H. M.: Capillary Hydrostatics and Hydrodynamics at Low G. Rep. No. LG-3, Stanford Univ., Sept. 1, 1964.

3. Otto, E. W.: Static and Dynamic Behavior of the Liquid-Vapor Interface During Weightlessness. AIChE Chem. Eng. Progr. Symp. Ser., vol. 62, no. 62, 1966, pp. 158-177.

4. Siegel, Robert: Effects of Reduced Gravity on Heat Transfer. Vol. IV., Advances in Heat Transfer. Academic Press, 1967.

5. Masica, William J.; and Petrash, Donald A.: Motion of Liquid-Vapor Interface in Response to Imposed Acceleration. NASA TN D-3005, 1965.

6. Harlow, Francis H.; and Welch, J. Eddie: Numerical Study of Large-Amplitude Free-Surface Motions. Phys. Fluids, vol. 9, no. 5, May 1966, pp. 842-851.

7. Masica, William J.; Petrash, Donald A.; and Otto, Edward W.: Hydrostatic Stability of the Liquid-Vapor Interface in a Gravitational Field. NASA TN D-2267, 1964.

8. Goodrich, F. C.: The Mathematical Theory of Capillarity. Parts I-III. Roy. Soc. Proc., ser. A, vol. 260, no. 1303, Mar. 21, 1961, pp. 481-509.

9. Rose, Walter; and Heins, R. W.: Moving Interfaces and Contact-Angle Rate-Dependency. J. Colloid Sci., vol. 17, 1962, pp. 39-48.

10. Friz, G.: On the Dynamic Contact Angle in the Case of Complete Wetting. Z. Angew, Phys., vol. 19, no. 4, 1965, pp. 374-378.

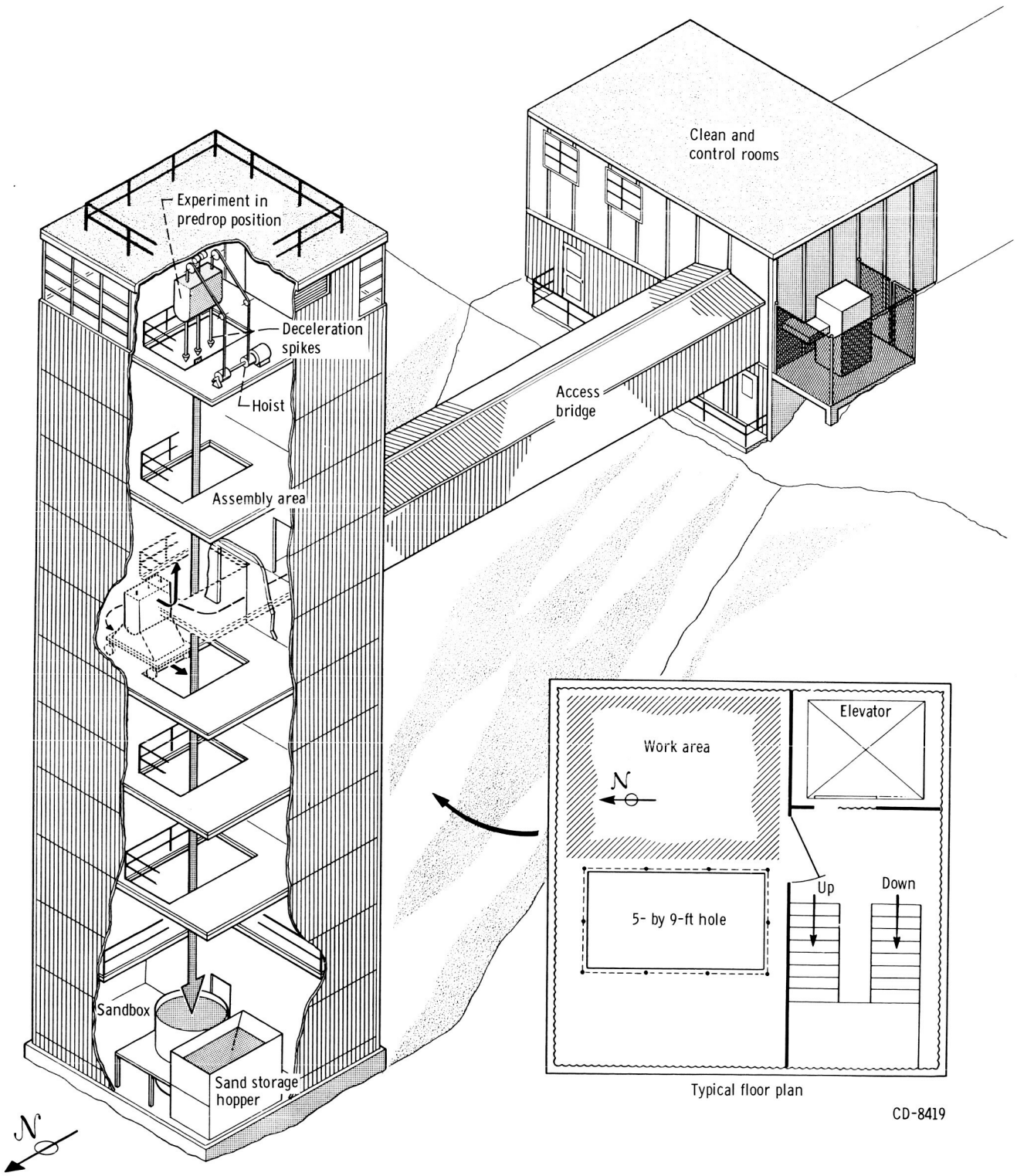

Figure 1. - 2.3-Second drop tower.

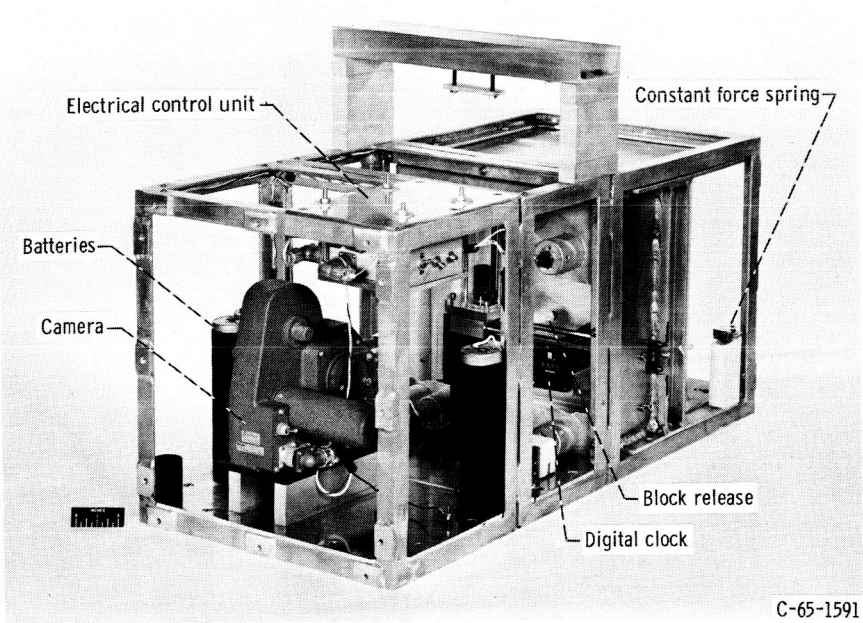

Figure 2. - Experiment package.

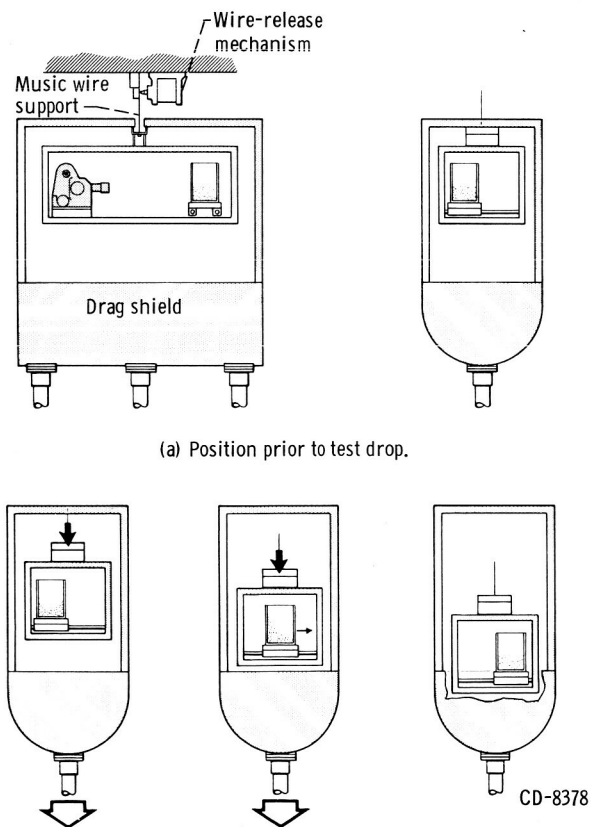

(a) Position prior to test drop.

(b) Free fall: formation of zero-gravity configuration.

(c) Application of lateral acceleration.

(d) Position after test drop.

Figure 3. - Schematic drawing showing sequential position of experiment before, during, and after test drop.

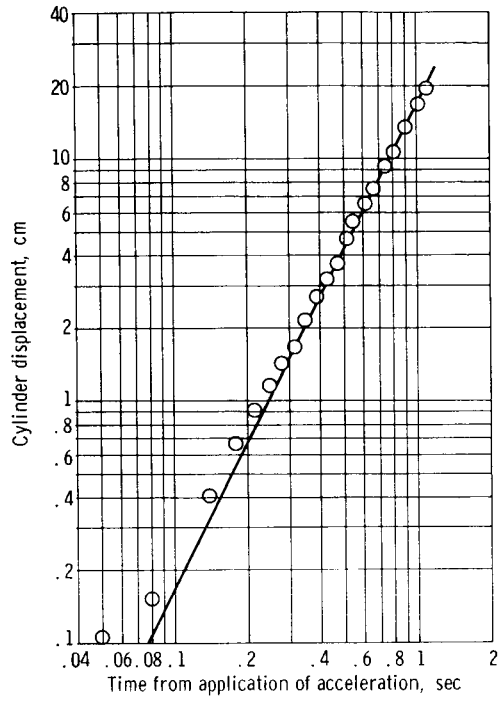

Figure 4. - Representative lateral acceleration characteristics using assumed slope of two. Lateral acceleration, 34 centimeters per second squared.

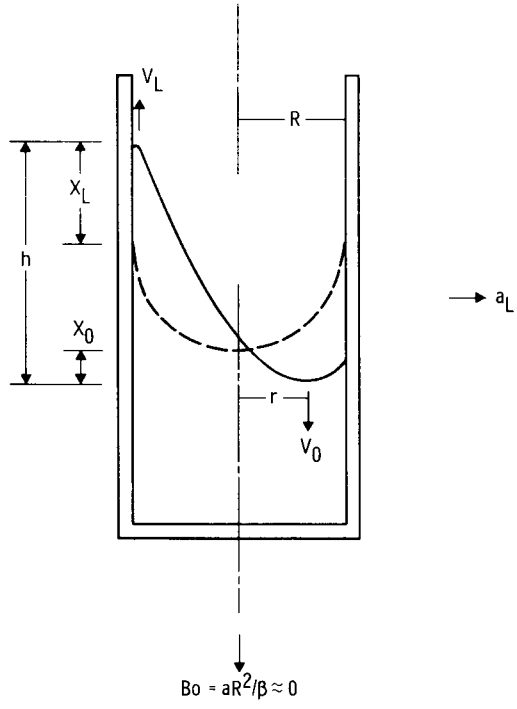

Figure 5. - Interface profile during lateral acceleration with zero axial Bond number.

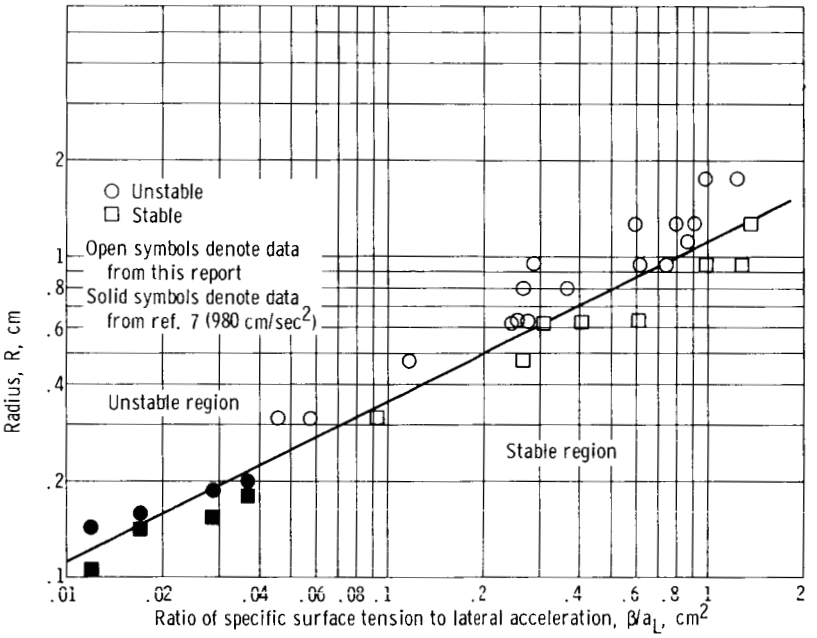

Figure 6. - Interface stability delineated by lateral Bond number.

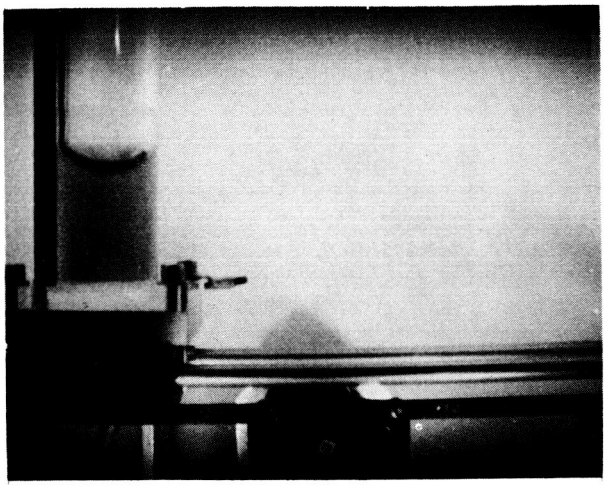

(a) Time, 0.01 second.

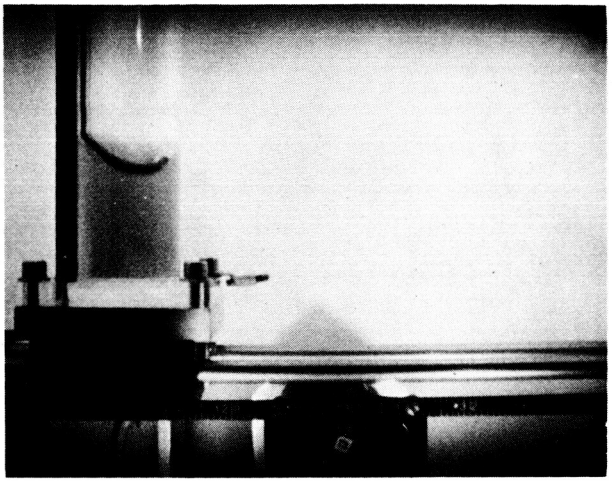

(b) Time, 0.11 second.

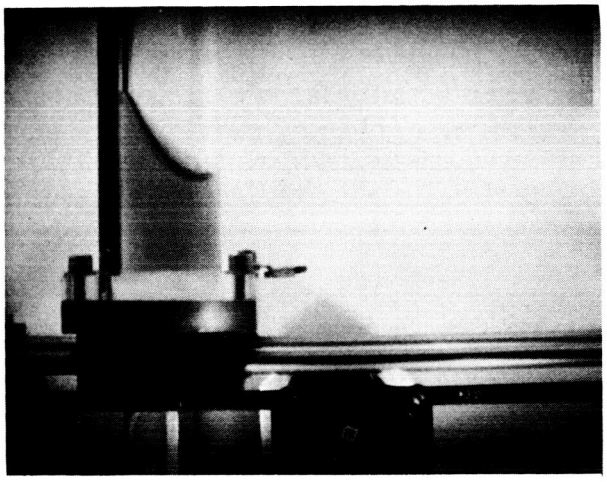

(c) Time, 0.31 second.

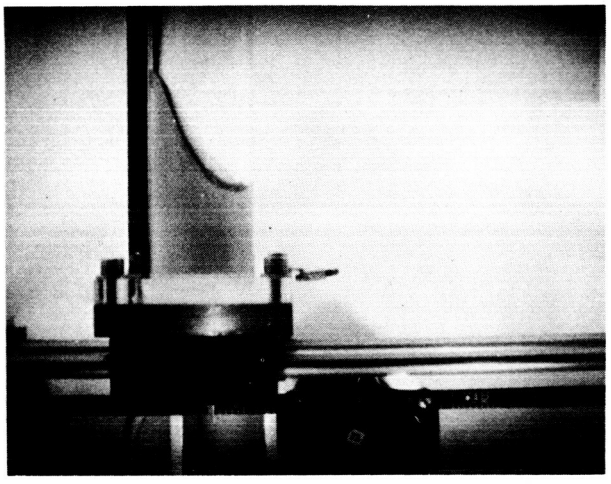

(d) Time, 0.41 second.

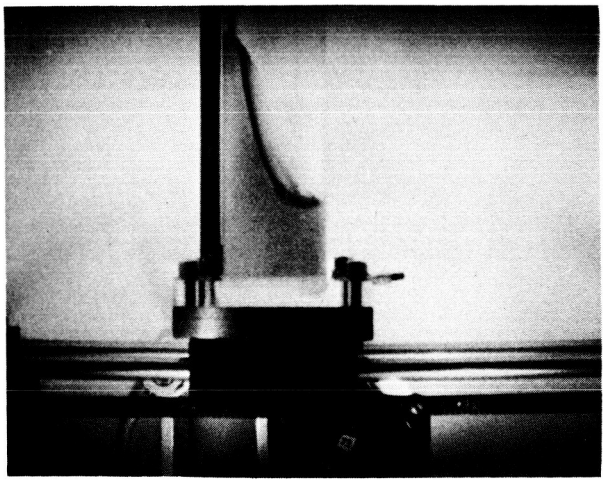

(e) Time, 0.61 second.

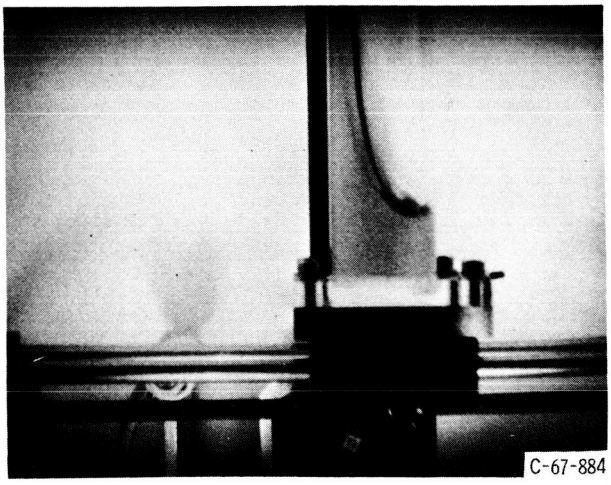

(f) Time, 0.81 second.

Figure 7. - Interface profile during representative run. Lateral Bond number, 3.7; cylinder radius 1.75 centimeters. Time measured following application transverse acceleration.

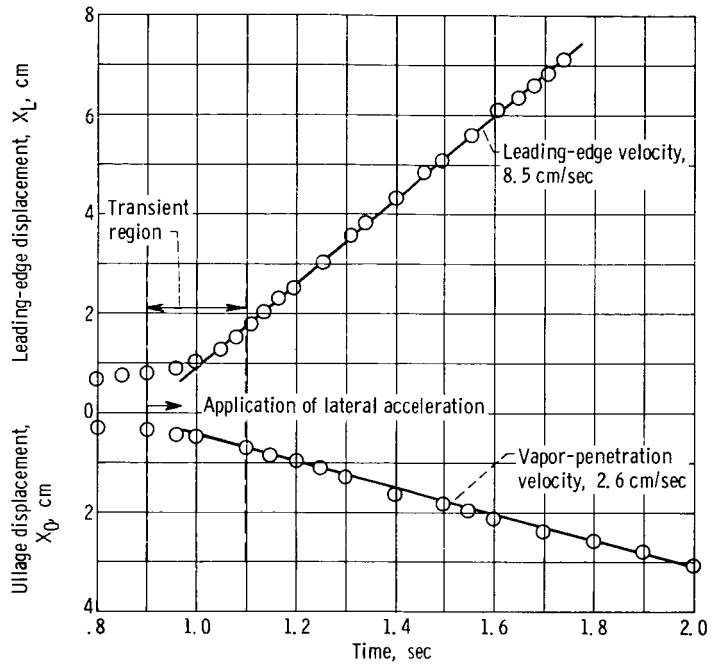

Figure 8. - Interface displacement during representative run.

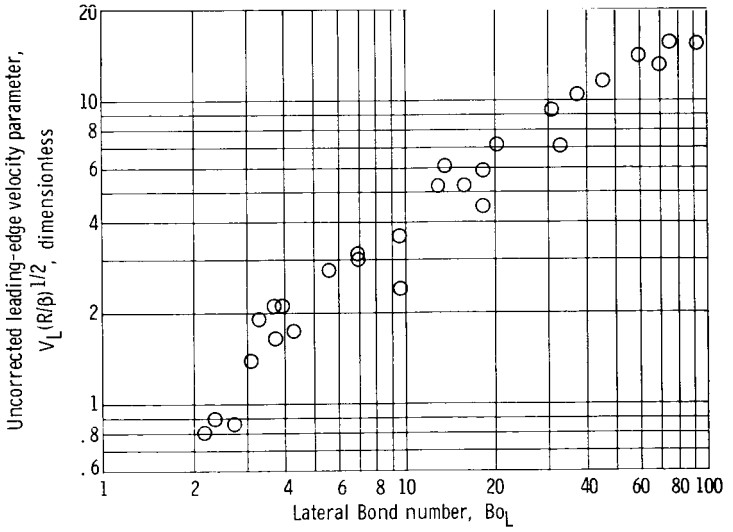

Figure 9. - Viscous effect on leading-edge velocity.

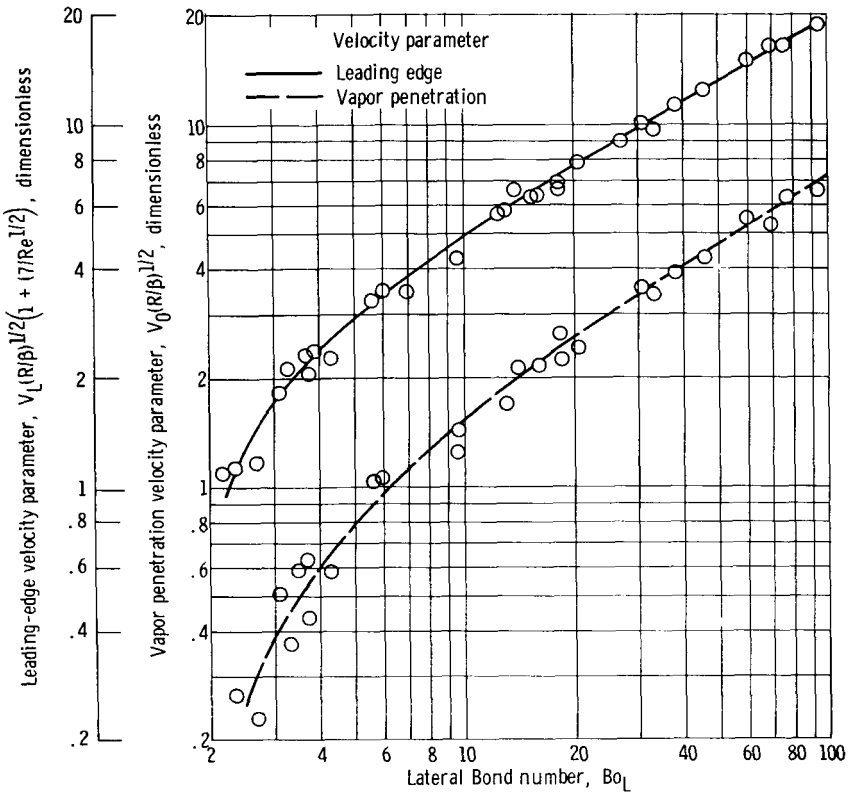

Figure 10. - Interface velocity parameters as function of lateral Bond number.

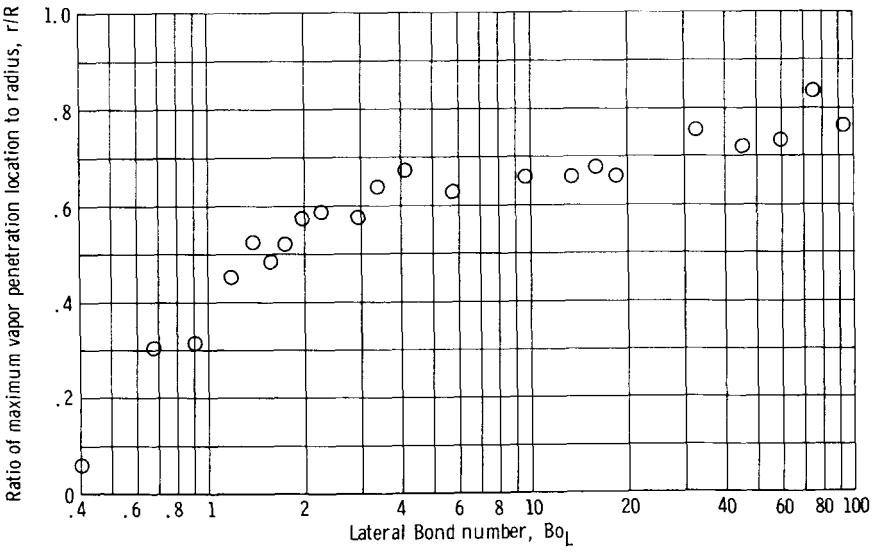

Figure 11. - Average steady-state horizontal location of vapor-penetration point.

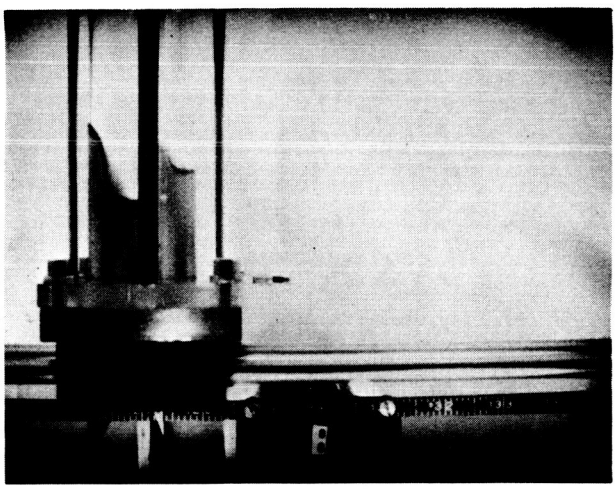

(a) At lateral acceleration cutoff.

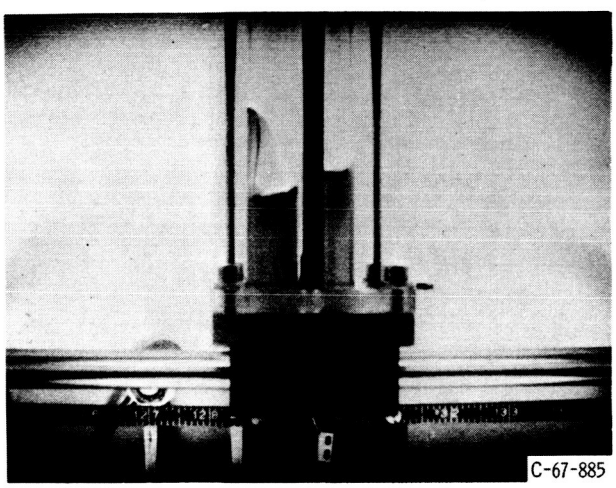

(b) Time after acceleration cutoff, 0.23 second.

Figure 12. - Interface behavior following lateral acceleration cutoff. Cylinder radius, 0.95 and 0.63 centimeter; lateral acceleration, 113 centimeters per second squared; specific surface tension, 28.3 centimeters cubed per second squared.

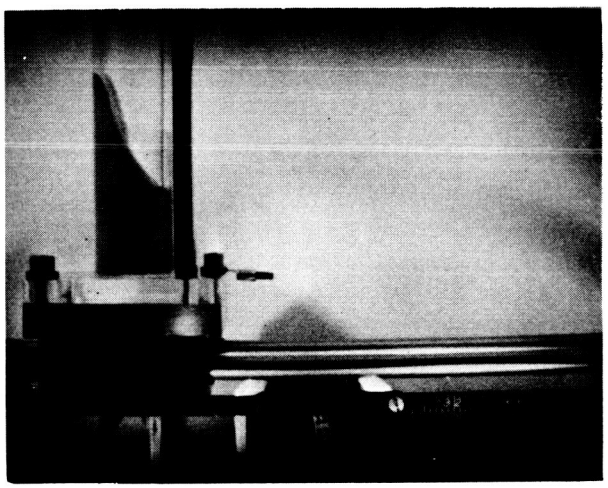

(a) At acceleration cutoff.

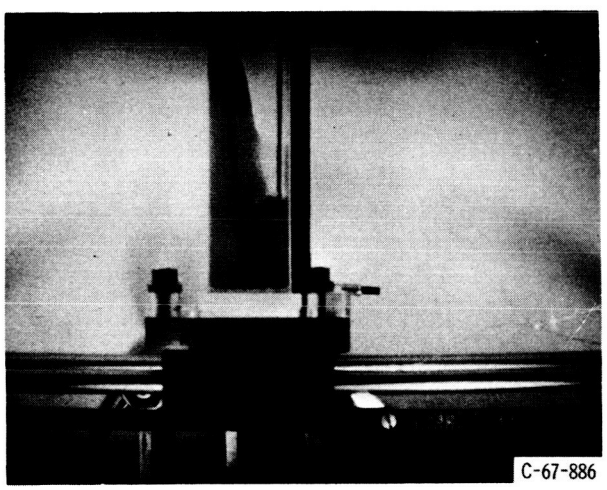

(b) Time after acceleration cutoff, 0.22 second.

Figure 13. - Interface behavior following acceleration cutoff. Cylinder radium, 1.27 centimeters; lateral acceleration, 119 centimeters per second squared; specific surface tension, 11.8 centimeters cubed per second squared.

(a) Time, 0.10 second.

(b) Time, 0.12 second.

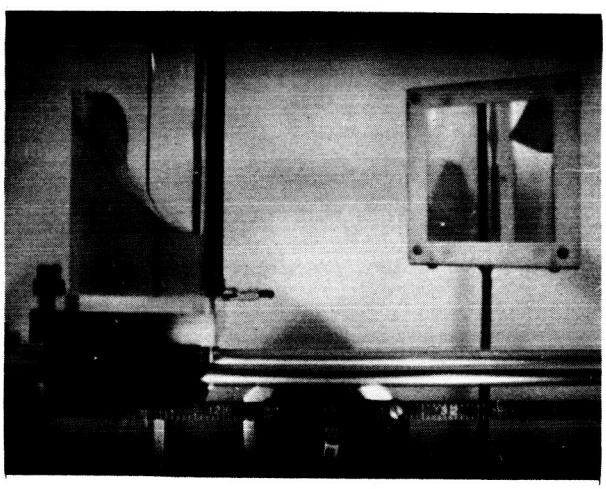

(c) Time, 0.14 second.

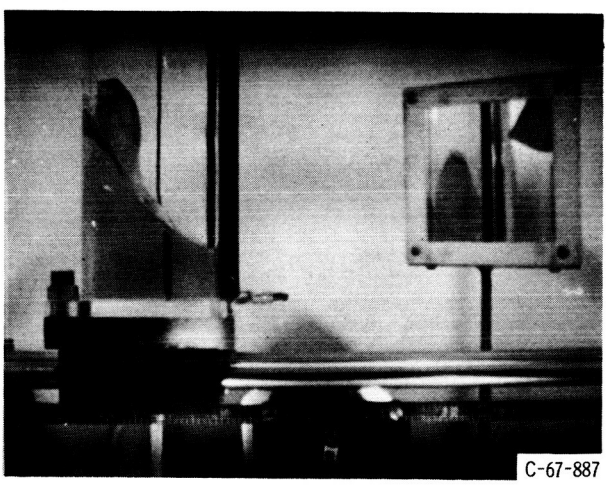

(d) Time, 0.16 second.

Figure 14. - Interface instability. Time measured after application of acceleration.